Eur. Phys. J. E (2017) **40**: 26
DOI 10.1140/epje/i2017-11514-8

THE EUROPEAN PHYSICAL JOURNAL E

Tips and Tricks

Formation of surface nanodroplets of viscous liquids by solvent exchange*

Brendan Dyett[1], Haitao Yu[1,2], and Xuehua Zhang[1,2,a]

[1] Soft Matter & Interfaces Group, School of Engineering, RMIT University, Melbourne, VIC 3001, Australia
[2] Physics of Fluids group, Department of Science and Engineering, Mesa+ Institute, and J. M. Burgers Centre for Fluid Dynamics, University of Twente, P.O. Box 217, 7500 AE Enschede, The Netherlands

Received 30 November 2016 and Received in final form 13 February 2017
Published online: 10 March 2017 – © EDP Sciences / Società Italiana di Fisica / Springer-Verlag 2017

Abstract. Surface nanodroplets are essential units for many compartmentalised processes from catalysis, liquid-liquid reactions, crystallization, wetting and more. Current techniques for producing submicron droplets are mainly based on top-down approaches, which are increasingly limited as scale reduces. Herein, solvent exchange is demonstrated as a simple solution-based approach for the formation of surface nanodroplets with intermediate and extremely high viscosity (1 000 000 cSt). By solvent exchange, the viscous droplet liquid dissolves in a good solvent that is then displaced by a poor solvent to yield surface droplets for the oversaturaion pulse at the mixing front. Within controlled flow conditions, the geometry of droplets of low and intermediate viscosity liquids can be tailored on the nano and microscale by controlling the flow rate. Meanwhile for extremely viscous liquids, the droplet size is shown to be dependent on the liquid temperature. This work demonstrates that solvent exchange offers a versatile tool for the formation of droplets with a wide range of viscosity.

1 Introduction

Microdroplets on surfaces are basic elements in a wide range of chemical, physical and biological processes, for example, for sensing, diagnosis, compartmentalized synthetic and catalytic reactions, and among many others [1–4]. The interest of stationary submicron-sized droplets originates from their very small volume, large specific surface area and long time stability [5]. Current techniques for producing submicron droplets are mainly based on top-down approaches by dividing a small volume of droplets from the bulk liquid, for example, via inkjet printing, parallel deposition by microfluidic robots [6], trapping droplets by microcavities, direct adsorption from emulsion droplets [7,8], or by splitting a mother drop on nanopatterns on the surface [9].

The top-down approaches are more difficult for droplets of femtoliter, due to the reducing nozzle size and increasing relevance of capillarity. It becomes extremely hard to deposit small and viscous liquids, due to the energy required to break up the droplet [10,11]. Physical stamps have been shown capable of depositing droplets of an increased viscosity [12] however are limited by the need for lithographic structures and the associated mechanical difficulties as scale reudces [13]. Methods such as matrix assisted pulsed laser evaporation [14] are also limited due to the requirement for specialized equipment. In bottom-up approaches, droplets may form by condensation, such as in dew formation [15,16]. However, condensation is only applicable to volatile liquids and requires control of a gaseous environment. Here we present a bottom-up approach of solvent exchange as a medium to produce nanodroplets liquids with negligible vapor pressure and extreme viscosity. The method is solution-based with simplicity, flexibility and scalability.

In this process, a good solvent (Solution A) of oil is displaced by a poor solvent (Solution B) in the presence of a substrate on which droplets of oil form, as sketched in fig. 1. A pulse of oil oversaturation is created at the mixing front of the two solutions during the exchange process. With coworkers, we recently reported the effects of flow and solution conditions on the droplet size [17–20], and established the scaling law between the droplet volume per unit surface area (Vol) and the Peclet number (Pe) during solvent exchange [17,21]

$$Vol \sim h^3 \left(\frac{c_{\mathrm{sat,poor}}}{\rho_{\mathrm{oil}}}\right)^{3/2} \left(\frac{c_{\mathrm{sat,good}}}{c_{\mathrm{sat,poor}}} - 1\right) Pe^{3/4}, \qquad (1)$$

where Vol, h, $c_{\mathrm{sat,poor}}$ and $c_{\mathrm{sat,good}}$ are the droplet volume, channel height, saturation concentration of oil in the poor

* Supplementary material in the form of a .pdf file available from the Journal web page at
http://dx.doi.org/10.1140/epje/i2017-11514-8

[a] e-mail: xuehua.zhang@rmit.edu.au

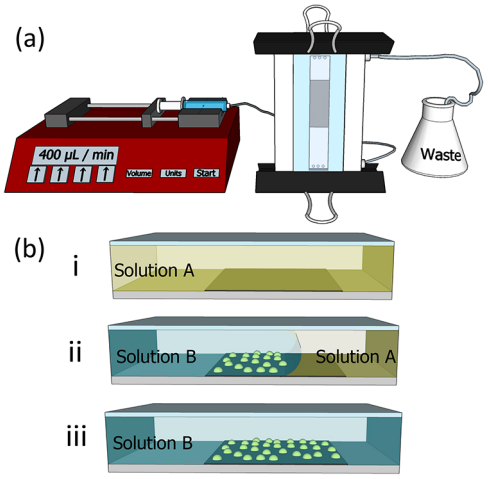

Fig. 1. (A) Schematic of the solvent exchange process. A syringe pump is used to control the flow rate, displaying a customizable flow rate of 400 μL per minute. A gas-tight syringe is connected via luer lock and teflon tubing to the inlet of the fluid cell containing a hydrophobic substrate. Similarly, waste is then directed by additional tubing from the outlet. (B) Schematic depiction of nanodroplet formation by solvent exchange. i) A fluid cell is charged with a good solvent, coined Solution A (pale yellow). ii) At a controlled flow rate, the solution is displaced by a poor solvent, coined Solution B (blue), nucleating surface droplets (bright yellow). iii) At completion, the fluid cell is fully charged with Solution B with stable surface nanodroplets across the substrate.

solvent and saturation concentration in the good solvent respectively. The Peclet number is defined by

$$Pe = \frac{Q}{wD}, \tag{2}$$

where D, Q and w are diffusivity of the solvent, flow rate and channel width, respectively. On prepatterned substrates, the droplet size can be tailored from nanometers to micrometers in height or from femtoliters to attoliters in droplet volume by varying the solution concentration or the base diameter of the chemical circular patterns [19,20].

Up to now, the solvent exchange process has been mostly applied to non-viscous droplets, including water, oils, or polymerisable monomers with viscosity ranging from 0.6 to 9 cSt [18,21]. In this work, we will demonstrate that solvent exchange is capable of preparing droplets with viscosity up to 1 000 000 cSt. Taking an example of siloxane polymer liquid, droplet size is shown to be dependent on flow rate and temperature. The finding of this study demonstrates the versatility of liquids that can be prepared as droplets by solvent exchange.

2 Experimental section

2.1 Chemicals and solutions

Polymethyhydrosiloxane (PMH) (M_n 1700-3200), Bis(3-aminopropyl) terminated poly(dimethylsiloxane) (Bis-amine (PDMS)) (M_n 2500), 2-hydroxy-2-methylpropiophenone (97%, Sigma), and 1,6-Hexanediol diacrylate (HDODA), were purchased from Sigma. Polydimethylsiloxane (PDMS) (DMS-T61, 1 000 000 cSt) was purchased from Gelest. Methyacryl-POSS cage mixture was purchased from Hybrid-Plastics. THF (AR, Chem-Supply), ethanol (AR, Chem-Supply), isopropanol (AR, Chem-Supply), sulfuric acid (97%, Chem-Supply) and hydrogen peroxide(30%, Chem-Supply) were used as received.

Table 1. Droplet liquids, viscosity, and the respective Solution A and Solution B for the droplet formation. The contact angles were measured by gently depositing the droplet liquid on the substrate immersed in Solution B.

Liquid	Mw [gmol^{-1}][a]	Viscosity [cSt]	Molecular structure	Solution A	Solution B	Contact Angle [°]
HDODA	226	9	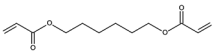	0.5 - 3 % in EtOH	Sat. H_2O	8 ± 1
PMH	1700-3200[a]	12-45	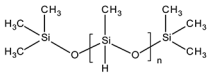	0.05 - 1% in IPA	H_2O	26 ± 5
Bisamine (PDMS)	2500[a]	50	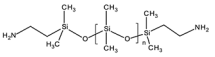	0.1 – 1 % in EtOH	H_2O	28 ± 4
Methacryl -POSS	1434	1,500	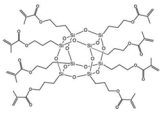	0.1 – 1 % in IPA	H_2O	51 ± 7
PDMS	300,0000[a]	1,000,000	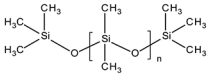	0.05 % in THF	H_2O	32 ± 7

(a) Number average, Mn.

For each liquid pair, a relatively good solvent, described as Solution A and a relatively poor solvent, described as Solution B were prepared as documented in table 1. To enable polyermization, a 0.2% solution of 2-hydroxy-2-methylpropiophenone was used as solution B. Where necessary, the solvent was saturated by thoroughly mixing the solute with water, upon thorough phase separation, the saturated water layer was then removed. In the case of HDODA and methacryl-POSS, upon completion of solvent exchange, the entire fluid cell was placed under UV to induce polymerization of the droplets.

To form droplets at elevated temperature, all syringes and solutions were preheated to the target temperature. The exchange was performed within a custom-designed fluid cell which was heated by a digitally controlled hot water bath. Before conducting the solvent exchange, the fluid cell was allowed to equilibrate by heating for 10 minutes.

2.2 Substrate preparation

A detailed guide for hydrophobic modification is available [22]. Briefly, a silicon wafer was placed in freshly prepared 3:1 piranha solution at 85 °C for 30 min. The wafer was then rinsed and sonicated in water and ethanol before drying under a stream of nitrogen gas. The wafer was held

above boiling water briefly until a breath figure appeared before being submerged in a freshly prepared solution of 1 mM octadecyltrichlorosilane in 8:1 hexane:chloroform for 20 min. The wafer was then consecutively rinsed and sonicated in hexane, acetone, ethanol before baking at 120 °C for 2 hours. Prior to use the wafer was cleaned by a high pressure stream of compressed CO_2, or "snow gun". This effectively removes particulate and organic contamination through momentum transfer and solvation, respectively [23]. The surface chemistry of silicon wafers employed were rendered hydrophobic by a SAM of trichloro(octadecyl)silane. In this case, the presence of moisture causes chlorosilanes such as OTS to undergo uncontrolled hydrolysis and polycondensation reactions leading to rough silica species.

2.3 Contact angle of sessile droplets

Contact angle measurements of the monomer droplets on OTS-Silicon were performed at room temperature (∼ 21 °C). The substrate was submerged within a quartz cuvette containing the respective Solution B. The contact angle was measured immediately after the droplet was deposited. For the highly viscous liquids, the droplet shape may be influenced by the deposition process.

2.4 Solvent exchange process

The substrate was placed inside a flow cell for the droplet formation. A schematic of the process and cell is described in fig. 1. A number of custom designed cells are also shown in the Supplementary Material in fig. S1. The materials for the container, spacer and tubing are compatible with the solvents and solute. The channel height was adjusted by the thickness of the spacer between the base and the top glass window. Physical maintenance of the seal of the cell was simply provided by binder clips. The flow rate of the second solution was controlled by the syringe pump (NE-1000, PumpSystems Inc.). After solvent exchange, surface droplets were observed by optical microscope in reflection mode (HUVITZ, HRM-300). For controlling the temperature during solvent exchange of highly viscous droplets, the custom designed cell in fig. S1a was used whereby a hot water bath was connected to the internal water circuit within the metal base.

3 Results and discussion

3.1 Droplet liquids with intermediate viscosity

Four oils of increasing intermediate viscosity (9–1500 cSt) were selected to initially test the possibility of solvent exchange to yield polymer surface droplets. A summary of the physical properties of the polymers used throughout this report is provided in table 1. In order of viscosity, they

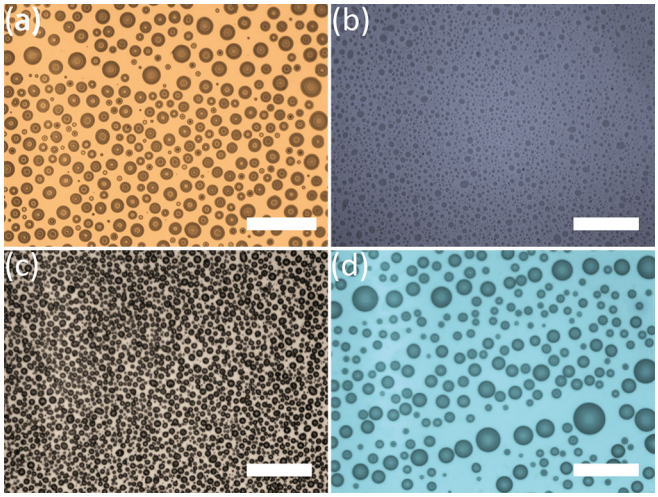

Fig. 2. Optical micrograph viewed in reflection mode of polymer droplets formed on a hydrophobic substrate. (a) Polymerized HDODA in air; (b) bisamine(PDMS) in water; (c) Methacryl-POSS in air; (d) PDMS 1 000 000 cSt in air. Scale bar = 50 μm.

are PMH (v = 15–45 cSt), bisamine(PDMS) (v = 50 cSt), and methacryl-POSS (v = 1500 cSt). After the solvent exchange under controlled conditions, many droplets of the viscous liquids were produced on the surface as shown in the optical images in figs. 2 and 3. The liquid, methacryl-POSS, could be polymerised, just like other polymerizable monomers reported in our previous work [24].

For a given concentration of the oil PMH (0.1% v/v), solvent exchange was performed at the flow rate from 200 μL/min to 1600 μL/min. The droplets formed are shown in fig. 3a-d. Clearly the droplet size becomes larger at a high flow rate. The quantitative analysis of respective droplet size is plotted in fig. 3e-h, showing that the mean droplet radius increases steadily from 3.7 μm to 6.1 μm with the flow rate from 200 μL/min to 1600 μL/min. As the radius increases, there is a general increase in polydispersity shown by the standard deviation and the broadening of the probability distribution function (PDF). Furthermore, the log-log plot demonstrates that the droplet volume per area scales with Peclet number with a power of 3/4. These results demonstrate that the scaling law $Vol \propto Pe^{3/4}$ holds for the formation of viscous polymeric droplets, same the formation of non-viscous droplets by solvent exchange in previous reports [17, 19–21, 25].

As the flow rate increases, the surface coverage also increases from 25% to 37%, while the number density decreases by a factor of ∼ 5. The inverse relationship between the surface coverage and the number density is expected, due to the enhanced droplet coalescence at high surface coverage. This collective interaction has recently been reported as universal for droplet formation by solvent exchange, independent of formation conditions [26]. The coalescence of droplets releases bare areas for the formation of new droplets, giving rise to the appearance of smaller droplets satellites around larger droplets.

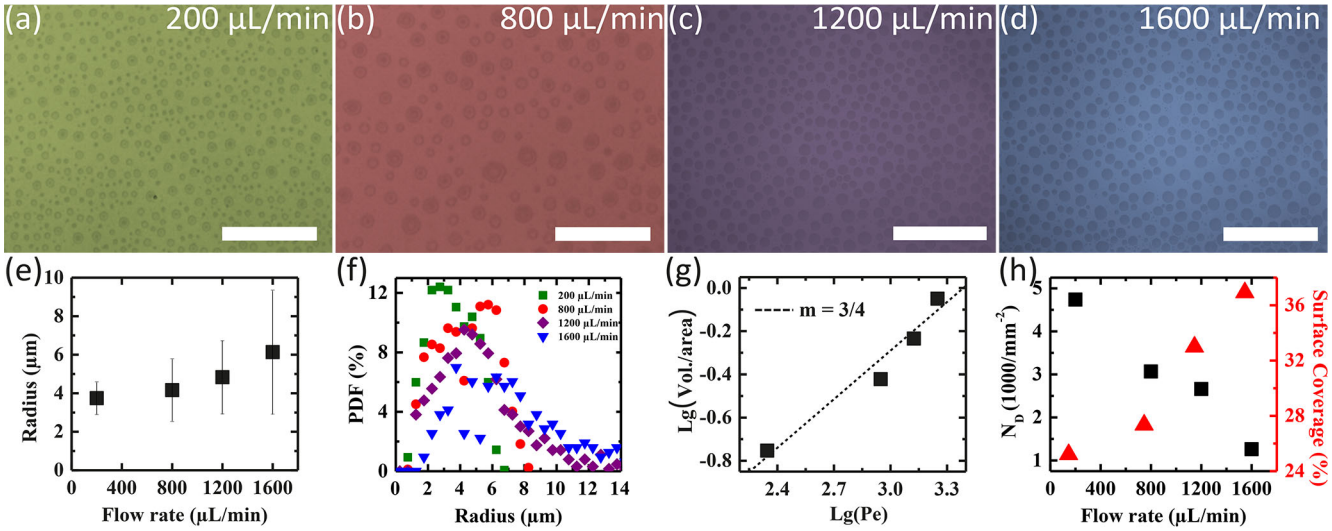

Fig. 3. (a-d) PMH droplets in water formed at flow rates 200, 800, 1200, 1600 μL/min, respectively. Scale bar = 50 μm. (e) Mean lateral radius and standard deviation of PMH droplets formed at various flow rates. (f) Number density (droplet count per mm^2) and surface coverage (%) with flow rates 200 μL/min (green square), 800 μL/min (red circle), 1200 μL/min (purple diamond) 1600 μL/min (blue triangle). (g) Plot of log[volume per area(μm^3/μm^2)] against log[Pe]; the dotted line indicates a gradient of 3/4. (h) Probability distribution function for (%) of droplet radius produced at different flow rates.

3.2 Droplet liquids with extremely high viscosity

PDMS with viscosity of 1 000 000 cSt was selected to further demonstrate the capability of solvent exchange for producing extremely viscous liquid droplets. A solution of PDMS in THF was exchanged by water. The droplets were observed after the solvent exchange performed at constant temperature of 22 °C with a flow rate of 1600 μL/min.

The PDF plot shows the droplet base radius is no more than 4 μm and the mean radius is around 2 μm. The formation of the polymeric droplets shows that the solvent exchange is a general approach for producing liquid droplets of a large variety. Viscosity of the droplet liquid is not a limiting factor for producing droplets by solvent exchange.

In an attempt to vary the droplet size, the flow rate was reduced by a factor of 4 from 1600 μL/min to 400 μL/min at 22 °C. There is only a slight decrease in the mean droplet radius to 1.9 ± 0.51 μm. These results suggest that the size increase of the extremely viscous droplets is limited with an increase in the flow rate at this temperature.

However, a dramatic increase in droplet size was observed as the solution temperature increased. As shown in the optical images in fig. 4, the mean radius increases from 2.17 ± 0.43 μm to 4.48 ± 1.52 μm as the temperature increases from 22 °C to 55 °C for the same concentration and flow rate. The surface coverage and the number density follow the universal inverse relationship: as the former increases from $\sim 17\%$ to $\sim 43\%$ with temperature, the latter drops by about a half.

Also of note, the surface coverage of 43% is higher than that typical of non-viscous droplets such as HDODA, possibly due to retarded coalescence between highly viscous droplets [27]. The droplet volume per unit surface area increases by almost one order of magnitude from 0.01 μm^3/μm^2 to 0.1 μm^3/μm^2.

Several physical properties of the solvent and solute vary with temperature that may influence the droplet growth. The viscosity is mainly determined by the non-viscous solvents, as the polymer solute is highly dilute. In the range of 22 °C to 50 °C, the dynamic viscosity of water decreases from 0.98×10^{-3} N s/m^2 to 0.6×10^{-3} N s/m^2 [28], while the diffusivity of the poor solvent and the polymer molecules in the poor solvent also increases [29–31]. However, it is likely that the effect of diffusivity is negligible, compared to the sharp decrease in droplet viscosity with temperature [32]. Moreover, the temperature dependence of the solubility of PDMS in solvents may also facilitate the formation of larger droplets [27].

Upon the formation, a liquid of such high viscosity is able to remain stable after the surrounding water is removed by a gentle stream of dry air, as shown in fig. 2d. The water front slides over the droplets without sweeping them off or causing them to merge, except that the base diameter of the droplets becomes slightly larger on the dry substrate, due to better wettability of PDMS in air. In contrast, non-viscous droplets or bubbles at a solid-water interface are mostly swept off or burst once water recedes [33, 34]. If required, ordered droplet arrays over a large surface area may be formed by using pre-patterned substrates, as demonstrated previously for non viscous liquids [19, 20, 35].

A final remark is that the formation of PDMS droplets by solvent exchange may have important implications for nanobubble research. Solvent exchange by using air-equilibrated ethanol and air-equilibrated water is often applied to produce nanobubbles on a solid surface. Misusing plastic syringes for such experiments has caused some misinterpretation of results from atomic force microscopy. The features were later proven to be PDMS droplets

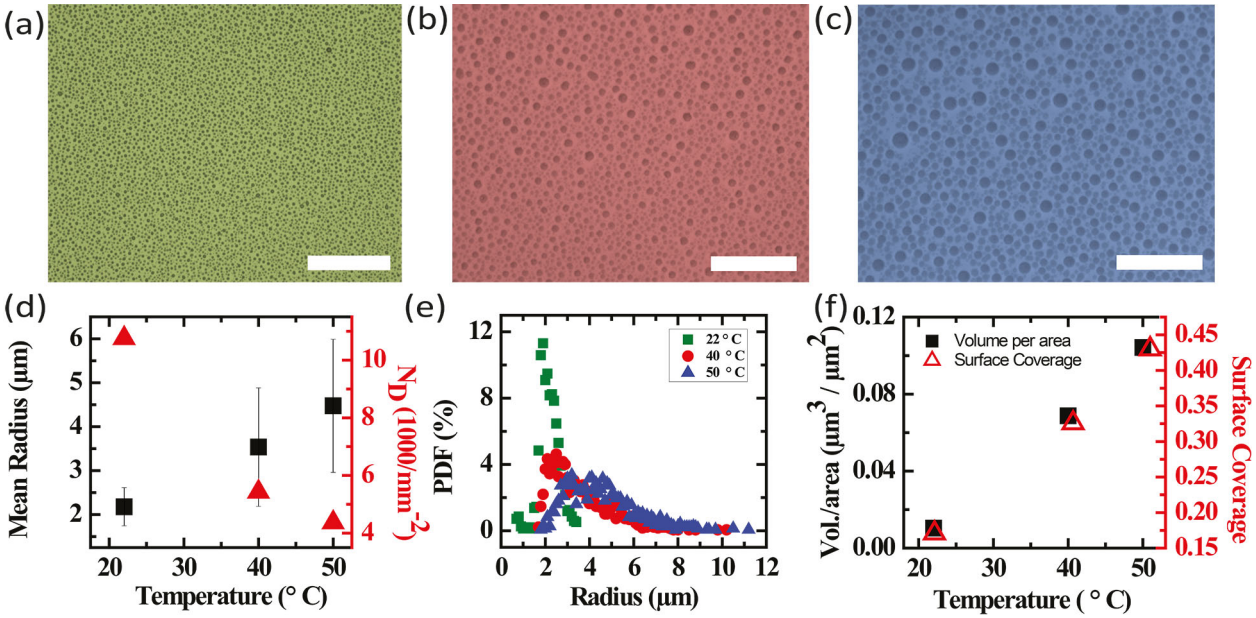

Fig. 4. (a-c) Optical micrograph viewed in reflection mode of submerged PDMS droplets at temperatures 22 °C, 40 °C, 50 °C, respectively. Scale bar = 50 μm. (d) Droplet radius (μm) size distribution of polymer droplets formed at 22 °C (green square), 40 °C (red circle), 50 °C (blue triangle). (e) Mean radius (μm) and number density (1000 s per mm^2) of droplets formed at three temperatures. (f) Volume per unit area (μL^3/μm^2) and surface coverage of droplets formed at three temperatures.

instead of nanobubbles. Recently, several approaches have been reported to distinguish PDMS droplets from nanobubles [36]. However, as shown in this work, the solvent exchange process can produce not only PDMS droplets, but also many kinds of liquid droplets. To confirm that the features are nanobubbles, it is therefore required to eliminate not only PDMS in nanobubble formation, but also all other liquid droplets. From this, it is suggested that the solvent exchange should be performed under clean conditions, by using clean ethanol and water, and glass containers and syringes and metal needles for handling the solvents.

4 Conclusions

The capacity of solvent exchange as a medium for droplet deposition has been extended from simple liquids to large molecular weight and highly viscous liquids. The viscosity ranges from 50 to 1 000 000 cSt. In contrast to other droplet deposition techniques, this work demonstrates that liquid viscosity is not a limiting factor for the droplet formation by solvent exchange. The volume of deposition could be tailored by the Peclet number for intermediate viscosity liquids. For high viscosity liquids, however, an elevated temperature was required to increase droplet deposition. Further work is required to develop a quantitative understanding of this temperature phenomena. The high stability of viscous droplets formed by this method may facilitate further research into interfacial phenomena. Moreover, the ability to prepare highly viscous droplets exemplifies the possibilities of future work with functional polymer droplets.

X.H.Z. acknowledges the support from Australian Research Council (FT120100473, DP140100805). We also acknowledge the use of facilities and the associated technical support at the RMIT MicroNano Research Facility (MNRF).

Author contribution statement

B.D. performed the experiments and prepared the manuscript, H.Y. assisted in data analysis, X.Z. conceptualized experiments and prepared the manuscript.

References

1. Jonathan Shemesh, Tom Ben Arye, Jonathan Avesar, Joo H. Kang, Amir Fine, Michael Super, Amit Meller, Donald E. Ingber, Shulamit Levenberg, Proc. Natl. Acad. Sci. U.S.A. **111**, 11293 (2014).
2. Hengquan Yang, Luman Fu, Lijuan Wei, Jifen Liang, Bernard P. Binks, J. Am. Chem. Soc. **137**, 1362 (2015).
3. Christopher A. Strulson, Rosalynn C. Molden, Christine D. Keating, Philip C. Bevilacqua, Nat. Chem. **4**, 941 (2012).
4. Jack W. Szostak, David P. Bartel, P. Luigi Luisi, Nature **409**, 387 (2001).
5. D. Lohse, X. Zhang, Rev. Mod. Phys. **87**, 981 (2015).
6. Ying Zhu, Yun-Xia Zhang, Wen-Wen Liu, Yan Ma, Qun Fang, Bo Yao, Sci. Rep. **5**, 9551 (2015).
7. Antonio Mendez-Vilas, Ana Belen Jodar-Reyes, Maria Luisa Gonzalez-Martin, Small **5**, 1366 (2009).
8. Haolan Xu, Xuehua Zhang, Adv. Colloid Interf. Sci. **224**, 17 (2015).

9. Huizeng Li, Qiang Yang, Guannan Li, Mingzhu Li, Shutao Wang, Yanlin Song, ACS Appl. Mater. Interfaces **7**, 9060 (2015).
10. Paul Delrot, Miguel A. Modestino, Franois Gallaire, Demetri Psaltis, Christophe Moser, Phys. Rev. Appl. **6**, 024003 (2016).
11. In Ho Choi, Joonwon Kim, Micro Nano Syst. Lett. **4**, 1 (2016).
12. Daeshik Kang, Changhyun Pang, Sang Moon Kim, Hye Sung Cho, Hyung Sik Um, Yong Whan Choi, Kahp Y. Suh, Adv. Mater. **24**, 1709 (2012).
13. Dinesh Chandra, Shu Yang, Acc. Chem. Res. **43**, 1080 (2010).
14. Alberto Piqu, Appl. Phys. A **105**, 517 (2011).
15. D. Beysens, C.M. Knobler, Phys. Rev. Lett. **57**, 1433 (1986).
16. Aijuan Zhang, Hua Bai, Lei Li, Chem. Rev. **115**, 9801 (2015).
17. Xuehua Zhang, Ziyang Lu, Huanshu Tan, Lei Bao, Yinghe He, Chao Sun, Detlef Lohse, Proc. Natl. Acad. Sci. U.S.A. **112**, 9253 (2015).
18. Ziyang Lu, Shuhua Peng, Xuehua Zhang, Langmuir **32**, 1700 (2016).
19. Lei Bao, Amgad R. Rezk, Leslie Y. Yeo, Xuehua Zhang, Small **11**, 4850 (2015).
20. Lei Bao, Zenon Werbiuk, Detlef Lohse, Xuehua Zhang, J. Phys. Chem. Lett. **7**, 1055 (2016).
21. Haitao Yu, Ziyang Lu, Detlef Lohse, Xuehua Zhang, Langmuir **31**, 12628 (2015).
22. M. Lessel, O. Bumchen, M. Klos, H. Hhl, R. Fetzer, M. Paulus, R. Seemanna, K. Jacobsa, Surf. Interfaces **47**, 557 (2014).
23. Robert Sherman, Drew Hirt, Ronald Vane, J. Vac. Sci. Technol. **12**, 1876 (1994).
24. Xuehua Zhang, Jingming Ren, Haijun Yang, Yuanhua He, Jingfung Tan, Greg G. Qiao, Soft Matter **8**, 4314 (2012).
25. Shuhua Peng, Detlef Lohse, Xuehua Zhang, ACS Nano **9**, 11916 (2015).
26. Chenglong Xu, Haitao Yu, Shuhua Peng, Ziyang Lu, Lei Lei, Detlef Lohse, Xuehua Zhang, Soft Matter **13**, 937 (2017).
27. W.D. Ristenpart, P.M. McCalla, R.V. Roy, H.A. Stone, Phys. Rev. Lett. **97**, 064501 (2006).
28. W.M. Haynes (Editor), *CRC Handbook of Chemistry and Physics* (CRC Press, 95 edition, 2014).
29. J.P. Munch, J. Herz, S. Boileau, S. Candau, Macromolecules **14**, 1370 (1981).
30. C.J.C. Edwards, R.F.T. Stepto, J.A. Semlyen, Polymer **23**, 865 (1982).
31. K.C. Pratt, W.A. Wakeham, Proc. R. Soc. A **336**, 393 (1974).
32. Gelest, Silicone fluids property profile guide. Technical report, Gelest Inc. (2012).
33. Xuehua Zhang, Henri Lhuissier, Chao Sun, Detlef Lohse, Phys. Rev. Lett. **112**, 1 (2014).
34. Chon U. Chan, Longquan Chen, Manish Arora, Claus-Dieter Ohl, Phys. Rev. Lett. **114**, 114505 (2015).
35. Haitao Yu, Shuhua Peng, Lei Lei, Ji Wei Zhang, Tamar L. Greaves, Xuehua Zhang, ACS Appl. Mater. Interfaces **8**, 22679 (2016).
36. Xingya Wang, Binyu Zhao, Jun Hu, Shuo Wang, Renzhong Tai, Xingyu Gao, Lijuan Zhang, Phys. Chem. Chem. Phys. **19**, 1108 (2017).